Modeling and simulation of high-speed cylindrical grinding based on 3D grinding wheel topography

IOP Conf. Series: Materials Science and Engineering **592** (2019) 012067 doi:10.1088/1757-899X/592/1/012067

Modeling and simulation of high-speed cylindrical grinding based on 3D grinding wheel topography

H P Chen [1], H Y Cao[1,*], R L Wu[1] and C Lu[1]

[1]State Key Lab of Digital Manufacturing Equipment & Technology, School of Mechanical Science and Engineering, Huazhong University of Science & Technology Wuhan 430074, PR China

*Corresponding authors: H Y Cao. E-mail address: hust-chy@foxmail.com

Abstract. The purpose of this paper is to establish a 3D virtual grinding wheel to illustrate the high-speed cylindrical grinding process of difficult-to-machine materials under various process parameters. Based on Monte Carlo method, the abrasive grain is modeled cutting spherical solid with random planes, and the random distribution of grains is obtained based on the virtual grid method. Then the grinding wheel topography is trimmed to adjust the protrusion height of abrasive grains. The simulations of high-speed cylindrical grinding under different grinding conditions are carried out considering the thermomechanical coupling effect of grinding wheel and workpiece. The 3D grinding wheel is validated by analyzing the grinding force ratio. The effects of cutting depth on the grinding performance, such as grinding force, workpiece temperature, effective stress and surface quality, are discussed. The results show that a smaller depth of grinding is beneficial for better surface quality.

1. Introduction

Different from regular tools, such as turning and milling cutters, grinding wheel is composed of irregular abrasive particles and bond. Because of the randomness of grinding grains' shape, distribution and protrusion height, it is difficult to study the actual grinding process and forecast the result. In order to accurately simulate the grinding process and forecast the grinding results, we need to establish a suitable grinding wheel model.

In general, the research of modeling and simulation of grinding processes is mainly concentrated on two aspects: single abrasive grinding and multi-grains grinding. Using a cone as a three-dimensional single abrasive grain, Chen et al. [1] simulated the whole process of diamond grinding, and analyzed the distribution of workpiece temperature and residual stress. Combining the Johnson-Holmquist 2 (JH-2) damage model, Liu et al. [2] simulated the generation and expansion of cracks in silicon carbide ceramics (SiC) single-grit grinding at different speeds. Fu et al. [3] studied the grinding force and stress distribution of single particle grinding Ti-6Al-4V by using a regular hexagonal abrasive grain with rounded corners. Taking into account the uneven grinding depth, Wang et al. [4] numerically studied the wear of CBN abrasive grains under high-speed grinding with regular hexagon abrasive grains, and then. The above studies simplified the abrasive grain with uniform regular shapes, and ignored the complicated interaction among multi-grains.

In the aspect of modeling and simulation of multi-grains grinding, Nguyen et al. [5] proposed a method to generate non-Gaussian grinding wheel topography ignoring abrasive grains modeling. Aurich et al. [6] established the grinding wheel topography based on the basic geometry (ellipsoid, tetrahedron, hexahedron, octahedron), and a kinematic simulation of the grinding process (KSIM) was developed.

Qiao et al. [7] simplified abrasive grains into pyramids and proposed a non-Gaussian statistical model to simulate the grinding wheel topography. Based on Aurich [6], Li et al. [8, 9] used the discrete element method to build a more realistic grinding wheel, being discontinuous with complex microscopic structure. Since the size, shape, protrusion height and distribution of the abrasive grains are not fully considered, the models established in the above studies differ from the actual grinding wheel topography.

In this paper, the method of random plane multi-cutting sphere is used to establish the grinding wheel profile which is in accordance with the actual distribution. At the same time, the high-speed cylindrical grinding is simulated by choosing the appropriate material constitutive, and the influence of different process parameters on the grinding quality is investigated.

2. Modeling procedure

As it's well known, the actual grinding wheel topography is complex and irregular because of the randomness of grains' shape, distribution and protrusion height. To simulate high-speed cylindrical grinding, we established a single grain model by cutting the sphere randomly based on Monte Carlo method. In addition, the virtual grid method is used to implement the random distribution based on the assumption of stochastic average distribution. Then adjust the protrusion height of the abrasive grains according to the actual distribution. Furthermore, a 3D virtual grinding wheel is generated by trimming the new grinding wheel. Finally, the grinding wheel is simplified to small rectangular blocks for the FEA geometric model according to the Saint Venant's Principle.

2.1. single grain model

The grain shape is usually modeled as sphere, pyramid, or regular polyhedron. Those simplified model can meet the simulation requirements to a certain extent, but most of the actual abrasive grains are irregular polyhedrons, and the simplified abrasive grains are far from the actual topography. In order to establish an actual abrasive grain, the method of cutting the sphere by random planes is adopted, as shown in the Figure 1(a). Figure 2 shows a single grain modeling process. The specific implementation steps are as follows:

1) Selecting grit designation and determining the diameter range $[D_{min}, D_{max}]$.

2) Taking a value D_0 randomly within the range $[D_{min}, D_{max}]$, and creating a solid sphere (A) of diameter D_0 with the origin $O(0, 0, 0)$ as the center of the sphere.

3) Taking a value D randomly with equal probability within the range $[D'_{min}, D_{max}]$, and creating a virtual ball (B) of diameter D with the origin $O(0,0,0)$ as the center of the sphere. In order to produce abrasive grains with a diameter of D_{min},$D'_{min}/2 = D_{min}/2 - (D_{max} - D_{min})/2$, that is to say, $D'_{min} = 2 * D_{min} - D_{max}$.

4) Taking a point P randomly on the surface of the virtual sphere B, and creating a tangent plane C by taking P as a tangent point. This tangent plane C divides the sphere A into two parts, and we delete the smaller part.

5) Repeating 3), 4) two steps in the appropriate times, and we can obtain a model similar to the actual abrasive grains.

By controlling the value of the initial diameter D_0, it is possible to obtain different sizes of abrasive grains that meet the particle size requirements. Figure 1(b) shows that the abrasive particles generated by dividing various times with ANSYS APDL. A large number of simulations show that the abrasive grains obtained by repeatedly cutting the initial sphere 45~55 times are most similar to the actual abrasive grains.

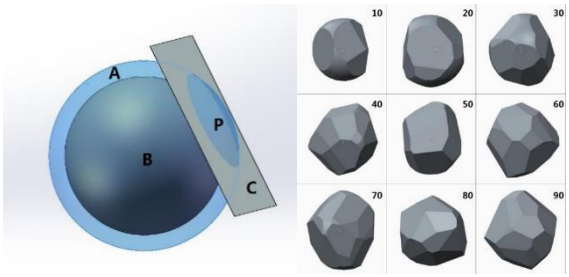

(a) (b)

Figure 1. cutting the sphere by random planes(a), grains obtained by dividing various times(b).

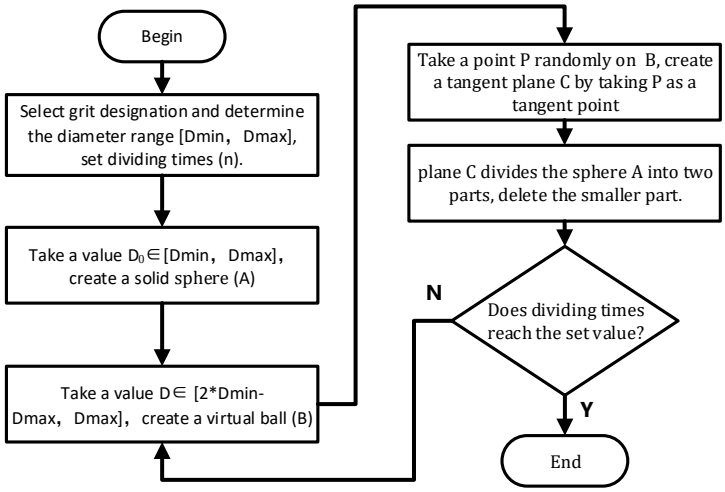

Figure 2. Flow chart of modeling single grain.

2.2. grinding wheel model

The actual grinding wheel topography is extremely complicated because of irregular abrasive particles. It is necessary to establish a model that conforms to the actual grinding wheel, then the randomness of size, distribution and height of the work should be achieved. A large amount of experimental data shows that for the same grit designation, the size of abrasives is in accordance with the Gaussian distribution[10]. Therefore, the initial diameter D_0 in the single grain modeling process should be selected in accordance with the Gaussian distribution.

The probability density function of the Gaussian distribution is

$$f(x) = \frac{1}{\sqrt{2\pi}\sigma}\exp\left(-\frac{(x-\mu)^2}{2\sigma^2}\right) \quad (1)$$

Where, μ is expectation, σ is standard deviation.

According to the pauta criterion, if the set $\{X\}$ conforms to the Gaussian distribution, taking any $x \in \{X\}$, the probability that the value x falls in $(\mu - 3\sigma, \mu + 3\sigma)$ is 0.9974. The diameter range of abrasive grains with 120# is [106mm,125mm], so the expectation of diameter is 115.5um, and the standard deviation is 3.167.

In practice, when the protrusion height of diamond abrasive grain exceeds 1/3 of its diameter, it is easy to break off during high-speed rotary grinding. For abrasive grain with a certain diameter D, we define the protrusion height ratio as proportion divided by the diameter. Therefore, the protrusion height ratio range is [0, 1/3]. Some researches show that the protrusion height of unused grinding wheel is in accordance with the Gaussian distribution [11]. According to the pauta criterion, the expectation and standard deviation of the protrusion height ratio can be calculated.

According to the expectation and standard deviation, a series of 120# abrasive grain diameters and the protrusion height ratio corresponding to the Gaussian distribution are generated based C++ program. The data generated results are shown in Figure 3.

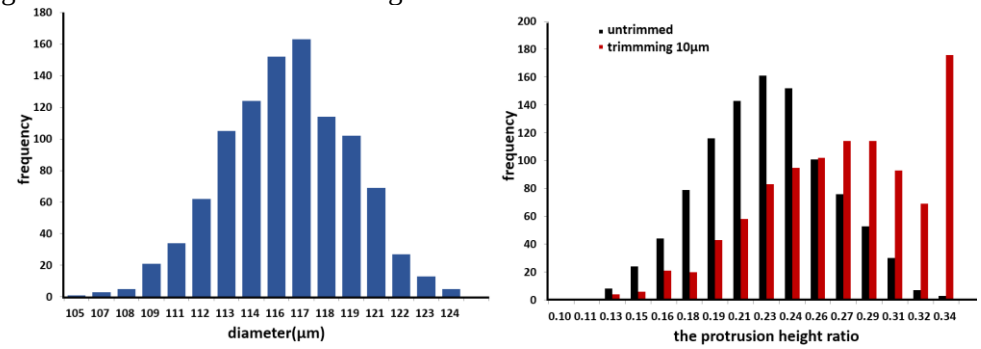

(a) (b)

Figure 3. The diameter distribution(a), the protrusion height ratio's distribution(b).

The distribution of abrasive grains on the grinding wheel is random. In this study, the assumption of stochastic average distribution is proposed, and a virtual grid method is employed to prevent interference between abrasive grains. As shown in the Figure 4, the surface of the grinding wheel is expanded into a plane and divided into several small squares of L*L (L is the average spacing of abrasive grains). The initial center of the abrasive grain is located at the center of the small square, and moved randomly with equal probability within the square to achieve random distribution of the abrasive grain. During the positioning of the abrasive particles, if interference with other abrasive particles occurs, the random number needs to be re-selected until there is no interference.

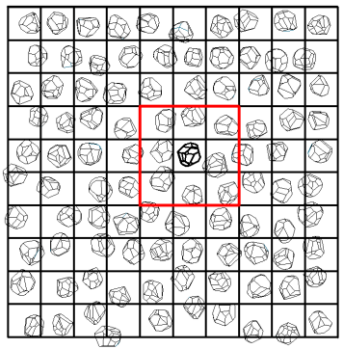

Figure 4. The distribution of grains on the surface of the grinding wheel.

As shown in the Figure 5, the above-mentioned randomly distributed abrasive particles are transferred onto the surface of the grinding wheel. The APDL is used to obtain the protrusion height H when the center of the sphere is distributed on the cylindrical surface. According to the protrusion height ratio file and grains' diameter file generated by the above C++ program, the protrusion height h corresponding to the abrasive grains can be obtained. Moving the center of abrasive grain radially to the grinding wheel by a distance of$h - H$, the protrusion height distribution can accord with Gaussian distribution.

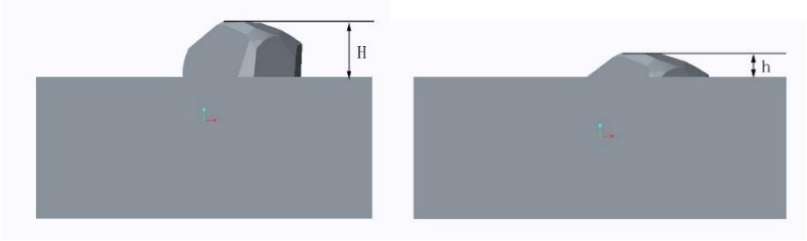

(a) (b)

Figure 5. The protrusion height before adjusting(a),the protrusion height after adjusting(b).

According to the above method, a grinding wheel model conforming to the actual new grinding wheel topography can be obtained. Figure 6(a) shows a grinding wheel block of 400 abrasive grains. The newly manufactured or worn wheel needs to be trimmed. As shown in the Figure 3, the protrusion height ratio after trimming 10μm accords with the Gauss distribution in the low region, and is evenly distributed in the high region. The overall protrusion height ratio is larger after correction. A 3D virtual grinding wheel block after trimming 10μm is shown in Figure 6(b). Figure 7 shows a grinding wheel model modeling process.

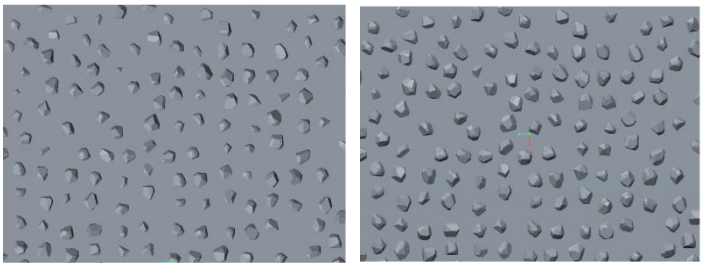

(a) (b)

Figure 6. The untrimmed model(a),the model after trimming 10μm(b).

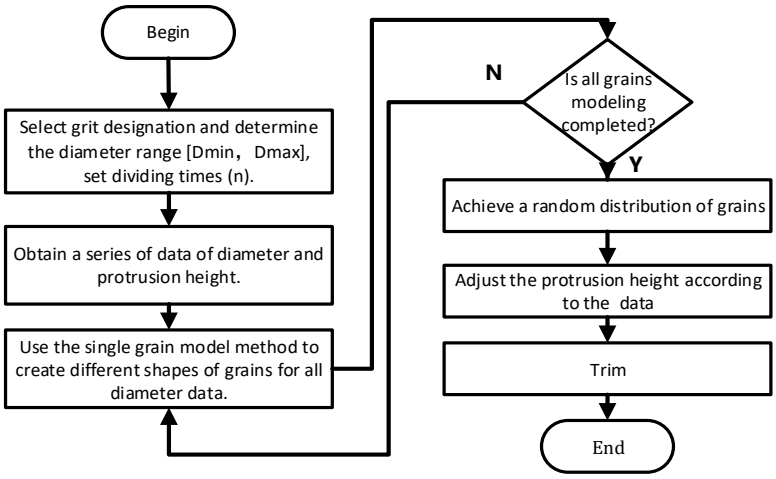

Figure 7. Flow chart of modeling grinding wheel.

2.3. Simulation model

According to the Saint Venant's Principle [12], the stress and strain of the workpiece are only concentrated in the grinding zone, so the stress and strain away from the grinding zone can be ignored. Therefore, the dimensions of the grinding wheel and workpiece can be simplified to small rectangular blocks for the FEA geometric model. This method can reduce the number of elements in the finite element simulation model and improve the simulation efficiency. The effective protrusion height is substantially greater than the grinding depth, so the interaction between the bonding agent and the workpiece is not considered in the simulation.

In this paper, $v_s = 45m/s, v_w = 20mm/s, D_s = 600mm, D_w = 40mm,$ the maximum grinding depth a_{pmax} is $0.038mm$, arc length is $1.2mm$.

Considering elastic deformation, the actual contact arc length is 1.3 to 2.3 times the theoretical contact arc length, the size of the grinding wheel block is 1.5*2 mm. The grinding wheel block has a total of about 260 abrasive grains, and the maximum protrusion height is 38um. Assuming that the maximum cutting depth is 30um, the thickness of the workpiece is 0.3mm. The final workpiece and grinding wheel block size is 1.5*2*0.3mm.

3. Simulation process

3.1. The selection of materials

In this paper, the diamond is selected for the grinding wheel and AISI-5140 for cylindrical workpiece. The material coefficients of diamond and AISI-5140 are shown in the following Table 1[1]. In fact, the deformation of the grinding wheel can be neglected and the deformation of the workpiece is larger. For this purpose, the rigid plastic finite method is applied.

Table 1. Material coefficients table.

Material	Density (Kg/m^3)	Young's modulus (MPa)	Poisson's ratio	Thermal expansion ($℃^{-1}$)		Thermal conductivity (W/(m °C))	
AISI-5140	7870	2 10000	0.277	20℃ 600℃	1.15e-5 1.61e-5	20℃ 600℃	35.5 25.5
Diamond	3520	900000	0.17	1.18e-6		2000	

In grinding process, the workpiece has the characteristics of high strain and high strain rate. The Johnson-Cook model takes into account the effects of temperature, strain and strain rate, and can represent the deformation characteristics of materials on the shear plane, so the J-C model is chosen as the material constitutive model of AISI-5140. The concrete expression of the model is as follows:

$$\sigma = (A + B\varepsilon^n)\left(1 + Cln\frac{\dot{\varepsilon}}{\dot{\varepsilon}_0}\right)(\frac{\dot{\varepsilon}}{\dot{\varepsilon}_0})^{\alpha}(D - ET^{*m}) \quad (2)$$

Where, $T^* = (T - T_0)/(T_m - T_0)$, $D = D_0 exp[k(T - T_b)^{\beta}]$.

The J-C model parameters of AISI-5140 are shown in the Table 2[1]:

Table 2. The J-C model parameters of AISI-5140.

A	B	C	D_0	E	n	m	α	β	$\dot{\varepsilon}_0$	T_0	T_m	T_b	k
894.1	763.6	0.06	1	1	0.35	1.5	0	0	0.002	20	1500	700	0

3.2. Friction type setting

In the grinding process, there are two kinds of contact situations: the contact between the grinding wheel and the workpiece, and the contact between the grinding debris and the workpiece. The friction type and value of these two contact situations are different. The friction type between the grinding wheel and the workpiece is defined as shear friction, and the friction coefficient is 0.5. The friction type between grinding debris and workpiece, grinding wheel and wear debris is defined as coulomb friction, and the friction coefficient is 0.3. As shown in the Figure 8.

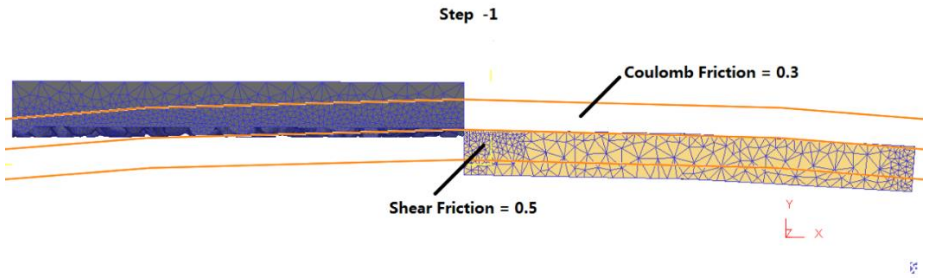

Figure 8. Friction type setting.

3.3. Boundary condition

In this paper, High-speed cylindrical grinding with inverse grinding is adopted. As shown in the Figure 9(a), taking the workpiece as a reference, the grinding wheel has two motions: rotation Vs and feed motion around the axis of the workpiece V_w. As shown in the Figure 9(b), it is assumed that the front (Z +), left (X -) and top (Y +) of the workpiece and the front, right and lower faces of the grinding wheel are in contact with the environment, and the remaining surfaces are the intercepted surfaces, which are not in contact with the environment. Therefore, the front (Z +), the left (X -) and the top (Y +) of the workpiece and the front, right and lower faces of the grinding wheel have heat exchange with the

environment, and the remaining faces of the workpiece are fixed in the X, Y, Z directions. The environment temperature is set as 20 °C and the convection coefficient is 1 N/s/mm/°C, and the heat-transfer coefficient among all the contact zones is 40 N/s/mm/°C.

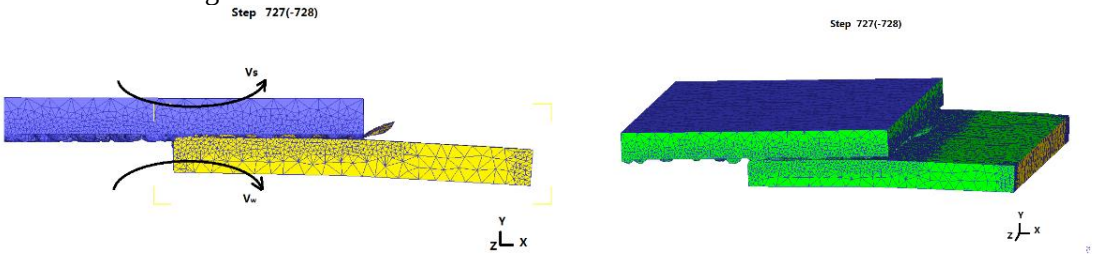

(a) (b)

Figure 9. The movement of grinding wheel(a), the heat exchange faces(b).

4. Results and discussion

Grinding wheel speed, workpiece speed, cutting depth, etc. are all parameters affecting the cutting quality. This paper focuses on the influence of cutting depth on grinding quality. The process parameters of simulation grinding are shown in the Table 3.

Table 3. The process parameters of simulation grinding.

Grinding speed v_s（m/s）	Workpiece speed v_w（mm/s）	Grinding depth a_p（μm）
45	20	10,20,25,30

In order to validate the model, the grinding force ratio is first discussed. The grinding force consists of three parts: normal grinding force, tangential grinding force and axial grinding force. The grinding force ratio, the ratio of normal force and the tangential force, is generally used to characterize the degree of difficulty of the abrasive particles pressing into the material surface. As shown in the Figure 10(a), the axial grinding force F_z is too small to be negligible in the grinding process; the variation trend of the normal grinding force F_y and the tangential grinding force F_x is the same, which is that the force increases first, then stabilizes and then decreases. This is because in the beginning stage, the effective abrasive grains increase and the cutting force increases with the continuous cutting of abrasive grains. Then it enters the stable grinding stage, and the abrasive grains cutting into and out of the workpiece keep dynamic balance, and the grinding force remains basically unchanged. In the final cutting stage, the abrasive grains continuously cut out and the grinding force decreases. As shown in Figure 10(b), most of the grinding force ratios are between 1.8~2.4, and this is consistent with Ref. [13]. This result proves the validity of the 3D grinding wheel modeling.

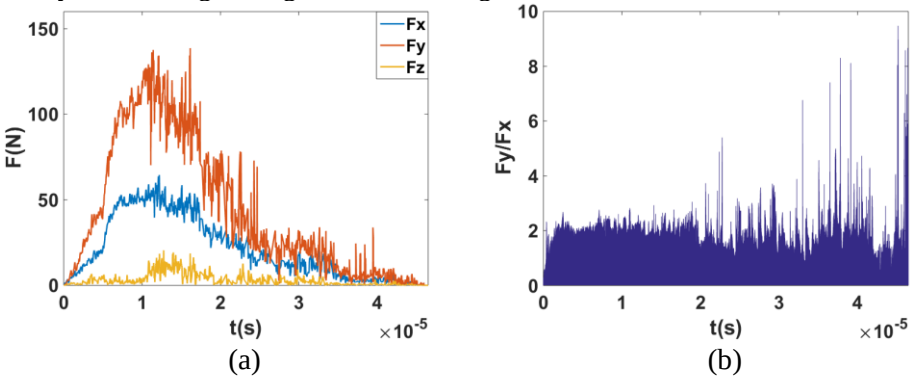

(a) (b)

Figure 10. The grinding forces(a), grinding force ratio analysis(b).

Figure 11 shows the maximum temperature history of workpiece. In Figure 11(a), the temperature distribution of the workpiece is showed. The temperature is less than the melting point (1400℃) in overall grinding zone, but in some areas, the temperature is larger than the melting point , where burn defects may occur. In order to research the temperature changes at different positions of the workpiece, four points on the same diameter of the workpiece were chosen, where P1-P3 are in the grinding layer

and gradually away from the surface, and P4 is below the grinding layer. As shown in Figure 11(b), in the grinding layer, the temperature will increase when the distance to the surface decreases, and the temperature change trend is consistent; in the area below the grinding layer, the temperature continues to rise.

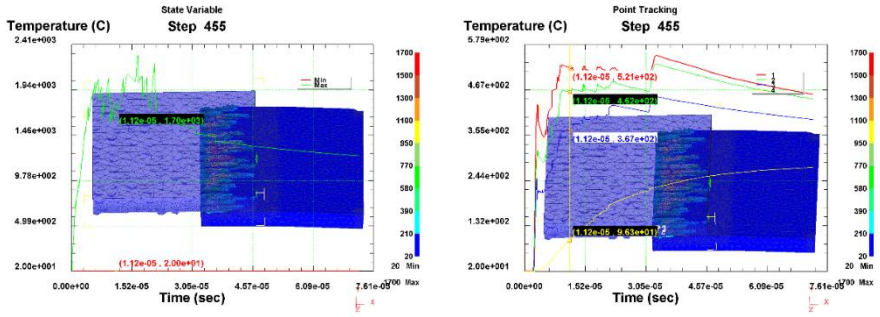

(a) (b)

Figure 11. The maximum temperature history(a), temperature history at different locations(b).

Figure 12 shows the effective stress distribution of workpiece. According to the graph, grinding has experienced four stages: A-B cut-in stage, B-C unstable grinding stage, C-D stable grinding stage, D-E cut-out stage. The minimum effective stress during the grinding process is always zero, and the surface has only tensile stress and no compressive stress. The maximum stress varies with the different grinding stages: in the A-B cut-in stage, the grinding wheel collides with the workpiece at high speed, and the maximum effective stress rises extremely rapidly; In the B-C unstable grinding stage, the continuous penetration of abrasive particles makes the workpiece upheave and form chips, the actual cutting depth increases continuously, and the maximum effective stress increases continuously. The theoretical cutting depth of cylindrical grinding increases firstly and then decreases with the cut-in and cut-out of abrasive grains. However, due to the influence of the upheaved workpiece and chips, the actual cutting depth in C-D stable grinding stage is basically stable, and the maximum effective stress fluctuates within a certain range. In the D-E cutting stage, due to the formation of the cutting mark, the last row of abrasive particles sometimes contact the workpiece and sometimes separate, and the maximum effective stress fluctuates sharply. After the complete cutting, the maximum stress becomes 0. Furthermore, the tensile strength σ_b of 40Cr is $980MPa$. As shown in Figure 10, the maximum effective stress of the workpiece in the grinding area is greater than σ_b. According to the theory of maximum tensile stress, brittle fracture occurs in the grinding area.

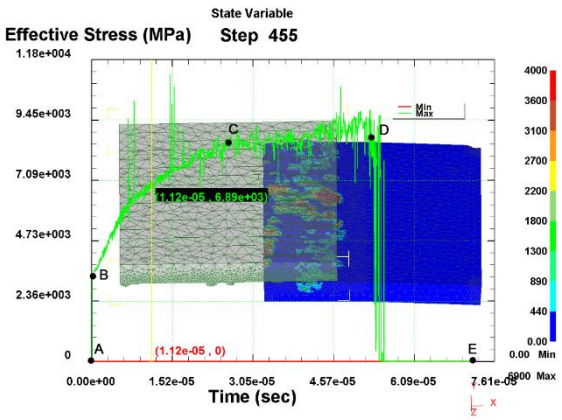

Figure 12. Analysis of workpiece's effective stress distribution.

In order to explore the influence of process parameters on maximum effective stress and temperature, grinding simulation was carried out under different process parameters. Figure 13 shows the maximum temperature and effective stress of workpiece at different grinding depths with the grinding speed of 45

m/s and workpiece speed of 20 mm/s. It can be seen that the maximum effective stress increases with the increase of the grinding depth at certain grinding speed. When the grinding depth reaches a certain degree, the maximum effective stress is independent of the grinding depth.

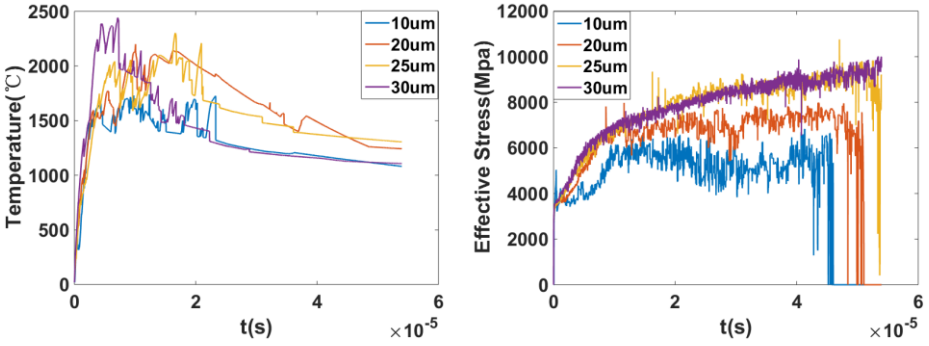

(a) (b)

Figure 13. Effect of different grinding depths

The surface of the workpiece after grinding can't be absolutely smooth. The surface roughness of workpiece surface is an important index to reflect grinding quality. Generally, there are two methods to evaluate surface roughness： arithmetical mean roughness (Ra) and maximum height (Rz), Ra can fully reflect the characteristics of workpiece surface profile, so Ra is preferred. Figure 14(a) shows the surface topography of the workpiece grinding surface at a grinding depth of 10μm. Figure 14(b) shows the arithmetical mean roughness Ra of the workpiece grinding surface with different grinding depths. The results show that the surface roughness of workpiece increases with the increase of grinding depth at a certain range of cutting depth.

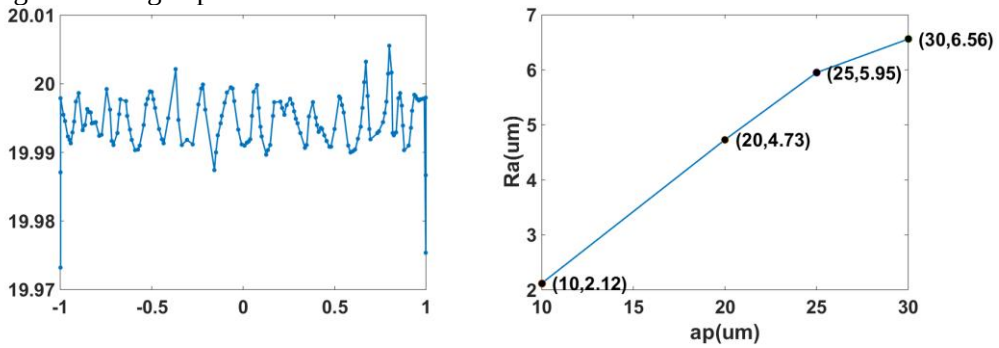

(a) (b)

Figure 14. The surface topography of the workpiece grinding surface

5. Conclusions

In this article， the grinding wheel model conforming to the actual grinding wheel topography is established by the method of cutting the sphere with random planes. The paper studies the grinding mechanism in high-speed cylindrical grinding through simulation. The following conclusions can be obtained:

(1) The method of cutting spherical solid by random planes can achieve the randomness of the size and topography of abrasive particles.

(2) Based on the spacing distribution of grains and the virtual grid method, a grinding wheel model which conform to the actual new grinding wheel topography can be obtained.

(3) Considering the thermomechanical coupling effect, the simulation of high-speed cylindrical grinding is carried out. The result of the grinding force ratio is consistent with the known conclusion, which can validate the proposed modeling method.

(4) The simulation of high-speed cylindrical grinding can reveal the effects of different process parameters on the maximum effective stress, defects, and surface quality.

Acknowledgments
This research is supported by the Science Challenge Project (No. TZ2018006-0102-03), the National Natural Science Foundation of China (No. 51875223) and the Doctoral Research Fund of Hubei University of Arts and Science (No. 2059023).

References
[1] Chen J, Fang Q and Zhang L 2014 Investigate on distribution and scatter of surface residual stress in ultra-high speed grinding *The International Journal of Advanced Manufacturing Technology* **75** 615-27
[2] Liu Y, Li B, Wu C and Zheng Y 2016 Simulation-based evaluation of surface micro-cracks and fracture toughness in high-speed grinding of silicon carbide ceramics *Int. J. Adv. Manuf. Technol.* **86** 799-808
[3] Fu D, Ding W, Miao Q and Xu J 2017 Simulation research on the grinding forces and stresses distribution in single-grain surface grinding of Ti-6Al-4V alloy when considering the actual cutting-depth variation *Int. J. Adv. Manuf. Technol.* **91** 3591-602
[4] Wang J, Yu T, Ding W, Fu Y and Bastawros A F 2018 Wear evolution and stress distribution of single CBN superabrasive grain in high-speed grinding *Precis. Eng.-J. Int. Soc. Precis. Eng. Nanotechnol.* **54** 70-80
[5] Nguyen T A and Butler D L 2005 Simulation of precision grinding process, part 1: generation of the grinding wheel surface *Int. J. Mach. Tools Manuf.* **45** 1321-8
[6] Aurich J C and Kirsch B 2012 Kinematic simulation of high-performance grinding for analysis of chip parameters of single grains *CIRP J. Manuf. Sci. Eng.-Trans. ASME* **5** 164-74
[7] Qiao G, Dong G and Zhou M 2013 Simulation and assessment of diamond mill grinding wheel topography *Int. J. Adv. Manuf. Technol.* **68** 2085-93
[8] Li H, Yu T, Zhu L and Wang W 2015 Modeling and simulation of grinding wheel by discrete element method and experimental validation *Int. J. Adv. Manuf. Technol.* **81** 1921-38
[9] Li H, Yu T, Zhu L and Wang W 2015 Analysis of loads on grinding wheel binder in grinding process: insights from discontinuum-hypothesis-based grinding simulation *Int. J. Adv. Manuf. Technol.* **78** 1943-60
[10] Hou Z B and Komanduri R 2003 On the mechanics of the grinding process – Part I. Stochastic nature of the grinding process *Int. J. Mach. Tools Manuf.* **43** 1579-93
[11] Hwang T W, Evans C J and Malkin S 2000 High Speed Grinding of Silicon Nitride With Electroplated Diamond Wheels, Part 2: Wheel Topography and Grinding Mechanisms *J. Manuf. Sci. Eng.-Trans. ASME* **122** 42-50
[12] Toupin R A 1965 Saint-Venant's Principle *Arch. Ration. Mech. Anal.* **18** 83-96
[13] Ren J X and Hua D G 1988 *Principle of Grinding* (Xi'an: Northwestern Polytechnical University Press)p 105